Lasers in Eng., Vol. 54, pp. 377–389
Reprints available directly from the publisher
Photocopying permitted by license only

Effect of Laser Power and Defocus on the Stability of Laser Welding 5083 Al Alloy with 5183 Al Alloy Filler Wire

S-G. HAN[1,2,*], Y-Q. YANG[1,*], B. YI[2], Z-Y. LUO[2], D-T. CAI[2], Y-F. XUE[2] AND X-H. REN[2]

[1]*School of Mechanical & Automotive Engineering, South China University of Technology, 381 Wushan Road, Tianhe, Guangzhou 510641, Guangdong Province, China.*
[2]*Guangzhou China-Ukraine Institute of Welding, Guangdong Academy of Sciences, 100 Xianlie Middle Road, Guangzhou 510650, Guangdong Province, China*
[3]*Yang Jiang China-Ukraine E.O. PATON Institute of Technology, Guangdong Welding Institute, 363 Changxing Road, Tianhe, Guangzhou 529500, Guangdong Province, China*

To clarify the influence of laser power density on the stability of laser welding 5083 Al alloy with 5183 Al alloy filler wire, experiments with different laser powers and levels of defocus, which are related to laser density, were carried out. A high speed camera, appearance inspection and macroscopic metallography were used to analyse the effects of laser power and defocus on the stability of welding wire melting, droplet transfer, molten pool fluctuation and weld solidification. The results showed that a small curvature curl would appear at the end of the wire if the laser power could evaporate the wire instantly. A large curvature curl would occur in the low power of the laser beam, which is too small to melt the wire. The droplet transition mode has gone through three stages of droplet transition liquid bridge transition→droplet transition, as the laser power was changed from 1600 to 2000 W, or the focus changed from -9 to +15 mm. Compared to the defocus, the laser power has a greater effect on the power density and the stability of the laser welding with filler wire. The droplet transition would occur when the diameter of the droplet exceeded the diameter of the wire. The weld metal surface had irregular flat areas periodically, while it was smooth during the liquid bridge transition. The violently fluctuating molten pool, splashes and holes would be appeared in the weld seam, when the molten pool had a high power density; however, when the molten pool had a low power density, asymmetric weld reinforcement would be found due to the small volume pool.

*Corresponding authors: E-mail: shanguohan@163.com (S-G. Han), meyqyang@163.com (Y-Q. Yang)

Keywords Disk laser, 5083 Al alloy, 5183 Al alloy, filler wire, laser welding, stability, power density, defocus, droplet transfer, weld formation

1 INTRODUCTION

Laser welding with filler wire is a promising welding method that can reduce the requirement for groove gap, change the chemical composition and improve laser utilization. In addition to being used in surface modification and additive manufacturing (AM) [1, 2], laser welding with filler wire can be used in dissimilar metal welding to achieve fine and thin welded joints with promising mechanical properties [3]. As is known, the stability of laser welding with filler wire is essential to achieving a favourable weld appearance and mechanical properties. Four aspects of welding wire melting, droplet transfer, molten pool flow, and solidification are included. Still, the laser welding of Al alloys has the characteristics of active plasma, high reflectivity and thermal conductivity [4, 5], which adds great difficulty to achieving the high-quality welded joints of Al alloys by using laser welding with filler wire.

It is of great significance to improve the stability of laser welding with filler wire by changing the beam energy distribution or preheating the welding wire. Compared with single-beam laser welding, dual beam laser welding has a lower energy density and heat accumulation effect. As a result, the appearance of the weld and the stability of the molten pool can be improved by using dual beam laser welding. The susceptibility to pores and cracks is reduced meantime [6]. The ring-shaped laser, shaped by Gaussian laser through a conical mirror and focused on the axis of the welding wire, can avoid splash caused by the evaporation of the metal vapour, and improve the stability of droplet transition [7]. Meanwhile, the introduction of new energy fields such as electromagnetic or electric arc is beneficial to increase the flow of the molten pool and improve the stability of the keyhole [8, 9].

The stability of laser welding with filler wire under different process parameters have been studied, including the relative position of the wire, the laser beam on the surface of the artifact, the wire feeding sequence, angle and feed rate, *etc*. In addition, the droplet transfer under different process parameters can be divided into two types, the liquid bridge transition and the droplet transition. The liquid bridge transition process is stable and the weld appearance is smooth; the droplet transition transfers liquid metal to the molten pool in the form of spaced droplets, accompanying splashes and poor appearance. The droplet transition mode is significantly affected by the force state of the droplet, especially for the state of the vapourised metal/plasma ejection force, which is closely related to the laser energy density [10, 11].

Previous studies on the stability of laser welding with filler wire are limited to a certain range of energy density and some stages of the welding process. It is difficult to reflect the stability of laser welding with filler wire as a

whole. So in the present study the relationship between the laser power density, related to laser power and defocus value, and the stability of the laser welding with filler wire have been studied by high speed camera, appearance inspection and macroscopic metallography. The mechanisms of the instability phenomenon under different energy densities have been clarified.

2 MATERIALS APPERATUS AND EXPERIMENTAL DESIGN

A schematic diagram of the experimental system for laser welding with filler wire is shown in Figure 1. In the welding process, the forward feeding wire, rear gas protection and a critical state between the laser beam and the wire on the surface of the test plate were adopted. The laser welding was conducted with a disk laser (TruDisk 10002; Trumpf GmbH) emitting a multimode beam at a wavelength of 1030 nm with a maximal power of 10 kW in continuous wave (CW) mode. The laser beam was conveyed by a 200μm diameter fibre to the welding head. The angle between the centreline of the laser welding head and the vertical line of the workpiece was 10° to avoid damaging the fibre from reflected laser light from the surface of the samples.

The materials choice in the experiments was 5083 Al alloy with the size of $100 \times 50 \times 3$ mm^3. The filler material feeding with the velocity of 2.0 m/min is a 5183 Al alloy wire with diameter of 1.2 mm, which keep the angle to the workpiece for 20°. The extension length of wire extending from the nozzle is set to 11 mm. The protective gas mask following the welding head

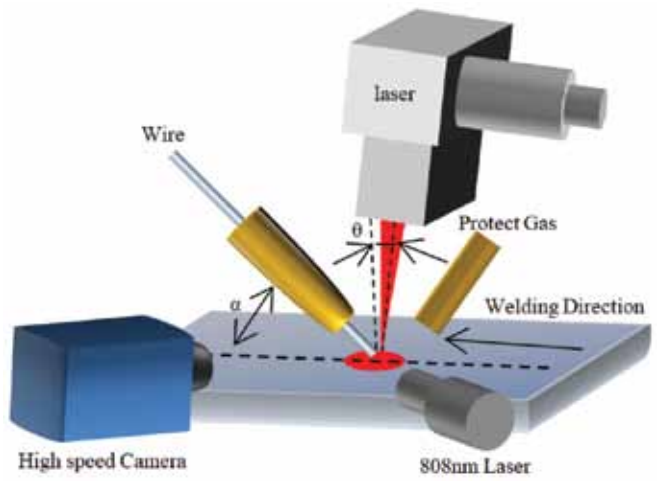

FIGURE 1
Schematic diagram of the experimental system configuration used for the laser welding with filler wire.

TABLE 1
The selected laser welding process parameters used in this work.

No.	P/W	f/mm	No.	P/W	f/mm	No.	P/W	f/mm
1-1	1800	-9	1-7	1800	+3	1-13	1800	+15
1-2	1800	-7	1-8	1800	+5	2-1	1400	-3
1-3	1800	-5	1-9	1800	+7	2-2	1600	-3
1-4	1800	-3	1-10	1800	+9	2-3	1800	-3
1-5	1800	-1	1-11	1800	+11	2-4	2000	-3
1-6	1800	+1	1-12	1800	+13	2-5	2200	-3

has been used to protect weld from oxidation with 99.999% Ar under a flow rate of 20 l/min. Before laser welding, organic matter such as oil is removed from the surface of the dual phase steel by nylon cloth with alcohol, while the oxide film on the 5083 Al alloy was polished by low power laser cleaning equipment.

In order to analyse the melting process of the 5183 Al alloy filler wire, the droplet transfer and the flow behaviour of the molten pool, a high speed camera system was built, which was composed of a high speed camera (pco.dimax cs4; Excelitas Technologies Corporation), a 808 nm wavelength diode laser (MDL-E-808; Changchun New Industries Optoelectronics Technology Company Ltd.) and a filter, zoom lens. The high speed camera sampling rate was 10,000 frames/s, resolution was 968 × 684 and the exposure time was 50 μs.

Two sets of process tests are designed in this paper: (1) When the laser power, P, is fixed at 1800 W, the defocus amount, f, varies from -9 to +15 mm, and (2) when f is set to -3 mm, the P varies from 1400 to 2200 W. The specific process parameters and weld formation are given in Table 1. The welding speed was maintained at 1.2 m/min.

3 RESULTS

3.1 Influence of laser power on stability

Figure 2 shows the droplet transfer behaviour and weld morphology as laser power is increased from 1400 to 2200 W. When P=1400 W the wire is only heated to a softened state, which is continuously curled with a large radius of curvature, under the direct action of the laser radiation. Part A in Figure 2(a) is the action point of the laser beam and the base metal (BM), while Part B is the crimped wire. An effective joint fails to be formed between the wire and the BM in this case. When P=1600 W or P=2000 W, the growth and transfer volume of the droplet are increased. The end of the wire shows coarsening

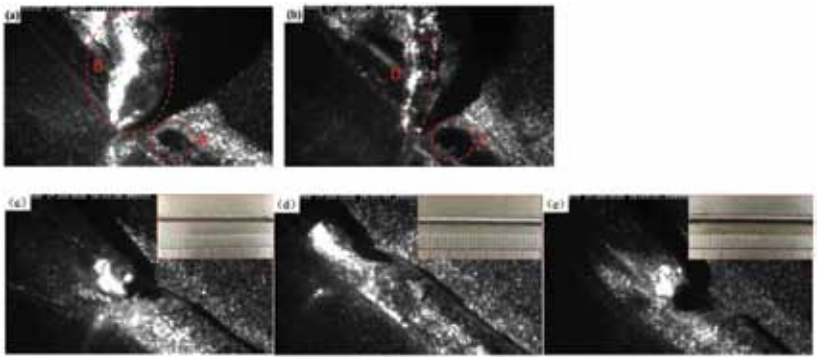

FIGURE 2
High speed camera still images of the droplet transfer behaviour and morphology of the welds under different laser powers of (a) 1400 W, (b) 2200 W, (c) 1600 W, (d) 1800 W and (e) 2000 W.

(see Figure 2(c) and Figure 2(e)). The transfer model of the droplet is liquid bridge transition mixed with droplet transition. When P=1800 W the melting of the wire and the transition of the droplet are in dynamic equilibrium. The transition model is liquid bridge transition and the weld surface is smooth. When P=2200 W the wire under the direct action of the laser is instantly vapourised. The subsequently fed wire is melted as it is close to the laser spot. The droplet at the end of the welding wire is curled with a small radius of curvature (see Figure 2(b)). Part C in Figure 2(b) is the action point of the laser beam and the BM. Part D is the crimped wire, and the wire and the BM are not effectively fused.

Figure 3 shows that for the well-formed welded joints, with the increase of the laser output wattage, the penetration and width of the weld seam are increased from 219.35 and 667.74 μm to 567.74 and 2110.75 μm, respectively, and the weld section is changed from the offset state to the symmetric state. The weld reinforcement is reduced from 840.86 to 641.94 μm. At the same time, the wettability and spreadability of the weld seam are improved and no porosity or holes have been observed on the weld section.

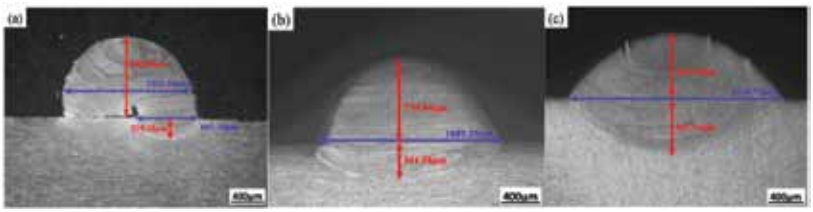

FIGURE 3
Optical micrographs showing the weld morphology obtained under different laser powers of (a) 1600 W, (b) 1800 W and (c) 2000 W.

3.2 Influence of defocus on stability

Figure 4 shows the droplet transition behaviour and appearance with different defocus. When +1 mm ≤f≤ +5 mm, although the droplet transfer mode is liquid bridge, a large amount of splashing can be find during droplet transition. The weld surface is poorly formed due to the severe fluctuation of the molten pool, as can be seen from Figure 4(d) to (f).

When -9 mm <f≤ +1 mm or +7 mm ≤f< +15 mm, the droplet will transition stably in liquid bridge mode with free splash (see Figure 4(b), Figure 4(c) and Figure 4(g)),and the surface of the weld is smooth because of small fluctuation of molten pool. While at f=-9 mm and f=+15 mm, the droplet appears droplet transition when the end of the weld is obviously coarsening and the surface of the weld is separated by bumps (see Figure 4(a) and Figure 4(i)). When f>+15 mm or f<-9 mm, the laser power density is too small to insufficiently melt the filler wire and the BM.

When the defocus changes from -9 to +15 mm, the weld penetration, width and reinforcement are change respectively by weakened W, strengthened W and ∧ (see Figure 5). When the defocus is -1 mm ≤f≤ +5 mm, the weld has a larger penetration and weld width, especially for f=+3 mm, the maximum penetration depth of 2606.52 μm and maximum weld width of 2970.30 μm are obtained, but there are holes left in weld seam and the weld cross-section is asymmetric. With the increase of defocus, the penetration,

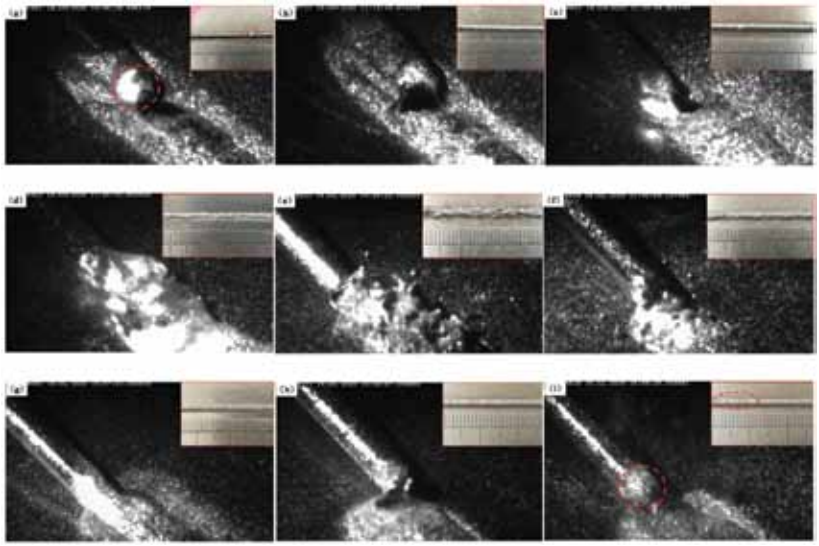

FIGURE 4
High speed camera still images of the droplet transfer behaviour and morphology of the welds under different defocusing amounts of (a) -9 mm, (b) -5 mm, (c) -3 mm, (d) +1 mm, (e) +3 mm, (f) +5 mm, (g) +7 mm, (h) +13 mm and (i) +15 mm.

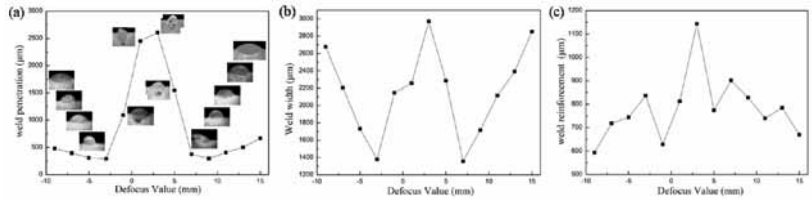

FIGURE 5
Graphs showing the effect of defocusing on weld formation for (a) penetration and cross-sectional morphology, (b) weld width and (c) weld reinforcement.

weld width and reinforcement are decrease rapidly, and the lowest value of penetration is about 290.0 μm when f=-3 mm and +9 mm, while the smallest weld width of 1370.0 μm appears at f=-3 mm and f=+7 mm, the holes disappear due to the stability of the keyhole became enhancement. When the defocus further increased, the penetration increases slightly, but the weld width increases rapidly. The weld cross-section is symmetrical, and most of the weld cross-sections are free of porosity and holes, except when f=7mm.

4 ANALYSIS AND DISCUSSION

As is known, when the power density received by the welding wire, E_{WV}, is greater than the upper limit the power density for stable surfacing, E_U, the wire under the direct irradiation of the laser beam will be instantly heated to the vaporisation temperature and then evaporated. The wire approaching the laser beam will be softened and a small curvature crimp appears. When E_{WV} is lower than the lower limit the power density for stable surfacing, E_D, the energy density is too low to melt the wire. The wire will be softened under the direct irradiation of the laser beam and produces a large curvature crimp. When the laser power density of E_{WV} is between E_D and E_U, the wire will be melted. After the droplet transition, the weld seam is formed on the BM. The laser power density received by the wire is lower than the E_D at the laser power of 1400 W, while that is higher than E_U when the laser power is 2200 W. When the laser power is between 1600 and 2000 W, the laser power density received by the wire is located between E_D and E_U. At -9 mm ≤f≤ +15 mm, the power density received by the wire is between the E_D and E_{WU} because no crimping of the welding wire has appeared; however, due to the sharp fluctuation of the molten pool, the power density received by the wire is close to the E_U when +1 mm ≤f≤ +5 mm.

When the power density received by the molten pool, E_{MV}, is greater than E_U, the temperature of the molten pool exceeds the boiling point. The molten pool fluctuates greatly, accompanied by splashing. After solidification, the weld seams with a rough surface, large penetration and width, are formed. If

the depth of the keyhole caused by the laser beam is too large, the keyhole can be divided into upper and lower parts, due to the instability of the sidewall. Because there is not enough solution to fill the lower part of the keyhole, a hole will be formed after the solidification of the molten pool.

When the E_{MV} is less than the E_D, the molten pool has the characteristics of small volume, fast cooling rate, and short solidification time; however, the large volume of the droplet expands on the surface of the BM after the droplet transition to form weld reinforcement. When the E_{MV} is between the E_D and the E_U, with the decrease of E_{MV}, the volume of the molten pool, weld penetration and width are all reduced. The flow of the molten pool is stable and no spatter. The surface of the weld seam is smooth after solidification. When the laser spot diameter is smaller than the diameter of the wire, the laser energy is used to melt the welding wire first, and then to melt the BM. When the laser power is 1600 W, the power density received by the molten pool is lower than the E_D. When the laser power is 1800 and 2000 W, the power density received by the molten pool is between the E_D and the E_U. Moreover, when -1 mm ≤f≤ +5 mm, the laser beam spot is so small that the energy density exceeds the E_U. The temperature of the molten pool exceeds the boiling temperature. When -9 mm ≤f≤ -3 mm or +7 mm ≤f≤ 15 mm, the power density received by the molten pool is between the E_D and the E_U; however, the laser beam diameter at the surface of the molten pool exceeds the diameter of the wire. Part of the laser energy directly acts on the BM. Then the width and depth of the molten pool are increased.

The growth and transition of the droplet are closely related to the force status of the droplet. Figure 6(a) shows that the forces include the gravity, F_G,

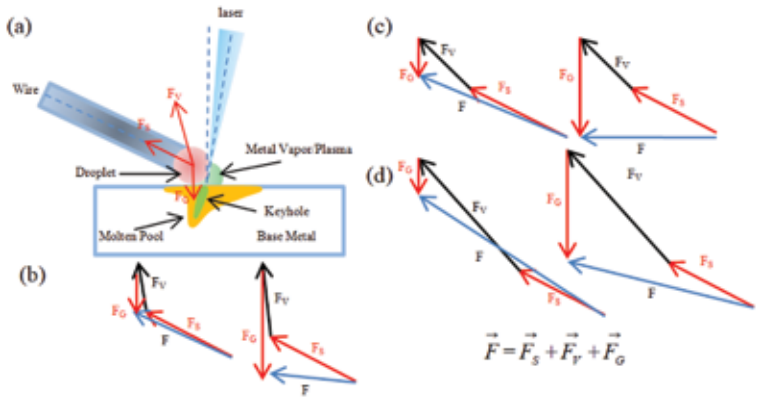

FIGURE 6
The force analysis of the droplet under different power densities: (a) schematic diagram of droplet force; (b) low laser power densities; (c) middle laser power densities; and (d) high laser power densities.

surface tension, F_S, and the metal vapour/plasma rebound force, F_V, [12]. Simplify the droplet to a spherical shape, then we have

$$F_G = \frac{4}{3}\pi r_d^3 \rho_d g \tag{1}$$

where r_d is the radius of the droplet, ρ_d is the density of the droplet, g is the gravitational constant and the direction of gravity is vertically downward. We also have

$$F_S = 2\pi r_w \sigma_w \tag{2}$$

where r_w is the radius of the welding wire, σ_w is the surface tension constant, and the direction of the surface tension is upward along the axis of the wire. Finally, we have

$$F_V = C_d A_p \left(\frac{\rho_p v_p}{2} \right) \tag{3}$$

where ρ_p is the density of the metal vapour, V_p is the velocity of the metal vapour, C_d is the tensile force constant related to the metal vapour and A_p is the projected area of the droplet force in the direction of its axis. And the rebound force of metal vapour/plasma is generated by the keyhole in the molten pool, which points upward on the droplet. The direction of the resultant force lies between the axis of the wire and the laser beam. As laser energy increases, the droplet contact area, the density, and the speed of the metal vapour are all increased. The direction of the resultant force strongly deviates from the axis of the wire [13].

From Equations (1) to (3) it can be seen that F_S remains constant. The F_G increases as the droplet size increases. And the F_V is positively correlated with the density, velocity, and size of the droplet. When the power density is low, both the velocity and density of the metal vapour are small (see Figure 6(b)) and so the value of F_V is small. The angle between the F_V and the laser beam is small. And the droplets continue to grow under the upward force. As the droplet diameter is equal to the diameter of the wire, both the F_G and the F_V become large; however, the direction of the resultant force keeps upward. The droplet still has the mechanical conditions to grow up. Eventually, the droplet coarsens at the end of the wire, and the droplet produces droplet transfer. With the increase of the laser power density the value of the F_V and the angle between the F_V and the laser beam are increased, as is evident from Figure 6(c). Before the size of the droplet reaches the wire diameter, the

direction of the resultant force on the droplet is parallel to the surface of the workpiece. The droplet growth and transition reach a dynamic balance, and the liquid bridge mode has appeared. When the laser power density further increases the value of the F_V and the angle between the F_V and the laser beam are increased rapidly, as one can see from Figure 6(d). The resultant force on the droplet is still upward even if the diameter of the droplet reaches the diameter of the wire. Then the volume of the droplet continues to increase without transition. The droplet becomes coarser, and finally droplet transition is produced.

The bubble, which simplifies into a spherical shape, escapes from the inside of the molten pool to the surface under the action of force in the liquid molten pool. The forces received by bubbles in the process include the upward buoyancy, F_F, surface tension, F_{S1}, and the fluid resistance, F_R, which hinders the movement of the bubble. From this we have

$$F_F = \frac{4}{3}\pi r_d^3 \rho_m g \tag{4}$$

where r_b is the radius of the bubble, ρ_m is the density of the solution and g is the gravitational constant. We also have

$$F_{S1} = 2\pi r_b \sigma_m \tag{5}$$

where σ_m is the surface tension constant of the molten pool. Finally, we have

$$F_R = \frac{1}{2} C \rho_m V^2 S \tag{6}$$

where C is the drag coefficient, V is the velocity of the bubble and S is the cross-sectional area of the bubble in the direction of movement.

The buoyancy of F_F is proportional to the cube of the bubble radius. The surface tension of F_{S1} is proportional to the bubble radius. And the fluid resistance of F_R is proportional to the square of the bubble overflow velocity and the bubble radius. The increase in the power density of the molten pool enhances the fluidity of the molten pool. It promotes bubble rupture and fusion, increasing the size of the bubble. The reason is related to the fact that the increment of buoyancy is much greater than that of the fluid resistance and surface tension. The direction of the resultant force is always upward, and the overflow time, T_P, is shortened. It can be concluded that the increase in the power density of the molten pool is conducive to the overflow of bubbles [14].

When the laser power increases, the molten pool solidification time, T_g, is prolonged, due to the increase in the bubble overflow distance. The residual probability of pores in the weld seam is reduced. When the defocus value is large, the heated area decreases on the BM caused by the laser directly. Then the energy density of the molten pool is low. The change of resultant force caused by the increase in the defocus value is small. The main influencing factor of the pores is the overflow distance, which leads to the formation of pores in the weld section when f=-7 mm; however, as the decreasing in defocus, the speed of bubble overflow can be increased, the pore overflow, T_P, will be shortened quickly, and the pore will disappear again [15, 16].

5 CONCLUSIONS

The influence of laser power density on the stability of laser welding 5083 Al alloy with 5183 Al alloy filler wire was ascertained through laser welding experiments with a disk laser using different laser powers and levels of defocus. In the process of increasing the laser power from 1400 to 2200 W, the filler wire has gone through five stages of large curvature crimping→end coarsening→stable melting→end roughening→end coarsening. Most of the laser energy is used to melt the welding wire when the laser power is low and an offset weld with a small molten pool left. Due to part of the energy of the large laser spot acts on the molten pool when the defocusing value change from -9 to +15 mm, the vapourised metal/plasma has a large rebound force and the wire has only three stages of end coarsening→stable melting→end coarsening. But when the focus radius on surface of wire is less than that of wire, the droplet transition and splashing of the molten pool are serious, an unstable keyhole resulting in holes in weld after solidification will form. The offset and uneven weld reinforcement will appear after violently fluctuating and solidification of the molten pool.

When the diameter of the droplet reaches the diameter of the filler wire, the resultant force is upward at low power density which fill with the mechanical conditions for droplet to grow up. The transition with droplet transition mode after the diameter of the droplet exceeds the diameter of the wire, and the surface of the welding seam is smooth. As the power density increases, the direction of the resultant force on the droplet is parallel to the surface of the workpiece at the condition of droplet size smaller than the wire diameter. A dynamic equilibrium that leads to the droplet transitions in a liquid bridge mode reaches between the droplet growth and transition, and the surface of the welding seam is smooth. As the power density is further increased, the resultant force is still upward even when the diameter of the droplet reaches the diameter of the filler wire, and the volume of the droplet continues to increase without transition. Eventually, the droplet that coarsens at the end of

the wire produces droplet transition , and the surface roughness of the weld is increased.

The increase of the energy density of the molten pool is beneficial to the flow of the molten pool and the fusion of the bubbles, which increases the resultant force on the bubbles, and the bubble overflow time is shortened. The molten pool solidification time and bubble overflow time change in the same direction as the laser power changing, and the probability of residual pores is low; while in the defocus changing, the fluctuation of bubble overflow speed caused by the variety of defocus is small when the molten pool is low energy density. The bubble overflow speed fluctuation caused by the change of the defocus is obvious when the energy density of the molten pool is high.

ACKNOWLEDGMENTS

For their support through financial funding. the authors thank Guangdong Academy of Sciences (GDAS) Project Sciences and Technology Development (2019GDASYL-0501011; 2018GDASCX-0803; 2021GDASYL-20210103085), Guangzhou Science and Technology Plan Projects (No.201907010006), the Guangzhou Economic and Technological Development Zone Science and Technology Plan Projects (No.2019GH19) and the Yangjiang Provincial Science and Technology Special Fund Project (SDZX2020007, SDZX2021010).

REFERENCES

[1] Sun X.F., Song W., Liang J.J., Li J.G. and Zhou Y.Z. Research and development in materials and processes of superalloy fabricated by laser additive Manufacturing. *ACTA Metallurgica Sinica* **57**(11) (2021), 1471–1483

[2] Wen P., Wang G. and Chen Y.Z. Effect of laser scanning and powder addition on microstructure and mechanical properties for hot-wire-feed laser additive manufacturing. *Journal of Laser Applications* **29**(2) (2017), 022302.

[3] Reimann W., Dobler M., Goede M., Schmidt M and Dilger K. Three-beam laser brazing of zinc-coated steel. *International Journal of Advanced Manufacturing Technology* **90**(1-4) (2017), 317-328.

[4] Chen Z., Ye H and Xu H.Y. Distortion control in a wire-fed electron-beam thin-walled Ti-6Al-4V freeform. *Journal of Materials Processing Technology* **258** (2018), 286–295.

[5] Aonuma M., Nakata K. Effect of calcium on intermetallic compound layer at interface of calcium added magnesium-aluminum alloy and titanium joint by friction stir welding. *Materials Science and Engineering B: Advanced Functional Solid-State Materials* **173**(1-3) (2021), 135-138

[6] Sonomura H., Ozaki T., Katagiri K., Hasegawa Y. and Tanaka T. Interface microstructure observation for welds of an alumina ceramics and an aluminum alloy with friction stir spot welding. *Journal of the Ceramic Society of Japan* **127**(2) (2019), 127-130

[7] Matjaz K., Makoto F., Gideon L and Levy G. Initial transient phase and stability of annular laser beam direct wire deposition. *CIRP Annals - Manufacturing Technology* **68**(1) (2019), 233-236.

[8] Meng X.M., Marcel B., Antoni A and Rethmeier M. Experimental and numerical assessment of weld pool behavior and final microstructure in wire feed laser beam welding with electromagnetic stirring. *Journal of Manufacturing Process* **45** (2019), 408-418.

[9] Xue J.Y., Li Y.X., Chen H and Zhu Z.T. Wettability, microstructure and properties of 6061 aluminum alloy/304 stainless steel butt joint achieved by laser-metal inert-gas hybrid welding-brazing. *Transactions of Nonferrous Metals Society of China* **28**(10) (2018), 1938-1946.

[10] Tao W., Yang Z.B., Chen Y.B., Li L.Q., Jiang Z.G. and Zhang Y.L. Double-sided fiber laser beam welding process of T-joints for aluminum aircraft fuselage panels: Filler wire melting behavior, process stability, and their effects on porosity defects. *Optics & Laser Technology* **52** (2013), 1-9.

[11] Jia Y.Z., Xiao J., Chen S.J and Huang W.H. Pulsed laser enhanced metal transfer of aluminum alloy in GMAW. *Optics and Laser in Engineering* **121** (2019), 29-36.

[12] Huang W.H., Chen S.J., Xiao J., Jiang X.Q. and Jia Y.Z. Investigation of filler wire melting and transfer behaviors in laser welding with filer wire. *Optics & Laser Technology* **134** (2020), 106589.

[13] Ma G.L., Li L.Q and Chen Y.B. Effects of beam configurations on wire melting and transfer behaviors in dual beam laser welding with filler wire. *Optics & Laser Technology* **91** (2017), 138-149.

[14] Galetto M., Genta G., Maculotti G and Verna E. Defect probability estimation for hardness-optimised parts by selective laser melting. *International Journal of Precision Engineering and Manufacturing* **21**(9) (2020), 1739-1753.

[15] Ba Y., Shi W.Q., Han S.G., Huang J.Y., Xie Y.P., Huang J and He K.F. Microstructure and mechanical properties of laser oscillated welded DP780 dual phase steel and 5083 aluminium alloy: Scanning oscillations at the same laser power . *Lasers in Engineering* **52**(1-3) (2022), 169-185.

[16] Ba Y., Shi W.Q., Han S.G., Huang J.Y., Xie Y.P., Huang J and He K.F. Microstructure and mechanical properties of laser oscillated welded DP780 dual phase steel and 5083 aluminium alloy: Scanning oscillations at the same energy density. *Lasers in Engineering* **51**(1-5) (2021), 299-313.